INSTITUTE OF PHYSICS PUBLISHING JOURNAL OF MICROMECHANICS AND MICROENGINEERING
J. Micromech. Microeng. **11** (2001) 153–160 www.iop.org/Journals/jm PII: S0960-1317(01)17236-0

On the out-of-plane deformation of V-shaped micromachined beams

ChingFu Tsou, Honglin Yin and Weileun Fang

Department of Power Mechanical Engineering, National Tsing Hua University, Hsinchu, Taiwan

Received 17 November 2000

Abstract
V-shaped beams are widely applied for the suspension of the sensors, fiber holders, and the suspension arms of atomic force microscopes. The performance of the V-shaped beam is highly dependent upon its initial out-of-plane deflection. This paper reports on the exploration of the out-of-plane deformation of V-shaped micromachined beams. A finite element model has been established to predict the deformation of a V-shaped micromachined beam. The fabrication and characterization of various shapes of SiO_2 V-shaped micromachined beams has been performed to observe the out-of-plane deformation caused by residual stress. With the difference between the analytical and experimental results, an etching process dependent mechanism has been discussed. Thus the design criteria to fabricate a flat V-shaped beam is accomplished.

(Some figures in this article are in colour only in the electronic version; see `www.iop.org`)

1. Introduction

Due to the restriction in silicon micromachining processes, there are a limited number of micromachined structures available. As shown in figure 1, micromachined cantilevers [1], bridges [2], and V-shaped beams [3] are the structures most commonly used to suspend microdevices. In this regard, a thermal isolation or a deformable micromachined structure can be obtained. Since the V-shaped beam has a high resonant frequency and larger torsional stiffness, it is widely applied to the suspension of sensors [4–6], fiber holders [7], and in atomic force microscopy (AFM) [8–10]. Unfortunately, these suspended micromachined structures are frequently deformed by thin-film residual stresses [11, 12]. For instance, a micromachined cantilever can be bent by the gradient residual stress [13] and a micromachined bridge can be buckled by the uniform compressive residual stress [14]. Thus, the performance of micromachined devices could be significantly affected [15–16].

The techniques to reduce the deformation of the micromachined structures induced by residual stresses have already been reported [17, 18]. In [17], thin-film residual stresses are reduced by modifying the deposition conditions. Another available approach is to compensate the net effect of the residual stresses using multi-layer thin films, for instance, the oxide–nitride bi-layer structure proposed in [18]. The previous approaches aimed at a reduction of the net thin-film residual stresses; however, their applications are limited by the available materials and fabrication processes. Hence, it is imperative to study the design rules of microstructures for

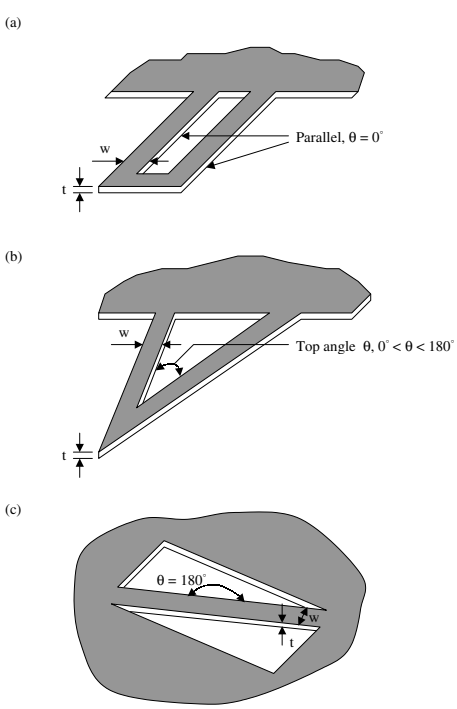

Figure 1. Three different micromachined beams (*a*) cantilever, (*b*) V-shaped beam, and (*c*) microbridge.

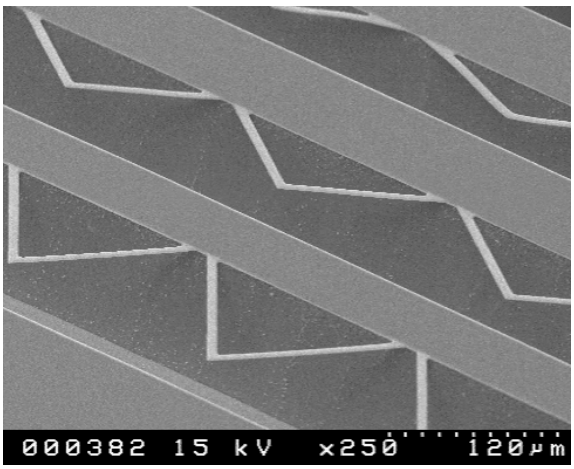

Figure 2. SEM photomicrograph of the V-shaped micromachined beams with various top angles θ.

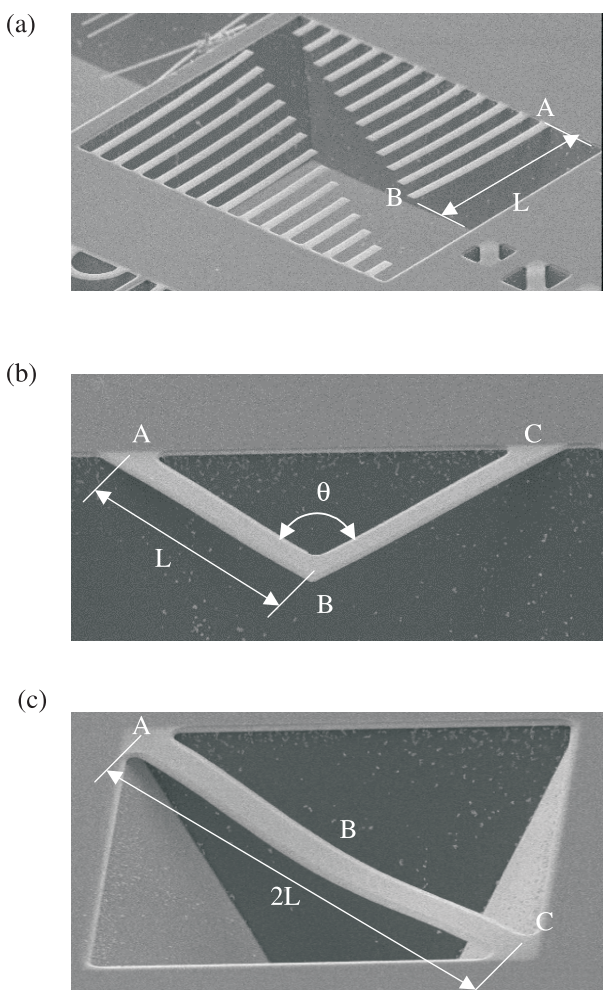

Figure 3. SEM photomicrograph of the micromachined beams fabricated in this study (*a*) cantilever, (*b*) V-shaped beam, and (*c*) microbridge.

reducing the out-of-plane deformation resulting from residual stress. The effect of residual stress on the deformation of microcantilevers [19, 20] and microbridges [14, 21] has been investigated extensively to date. On the other hand, there is

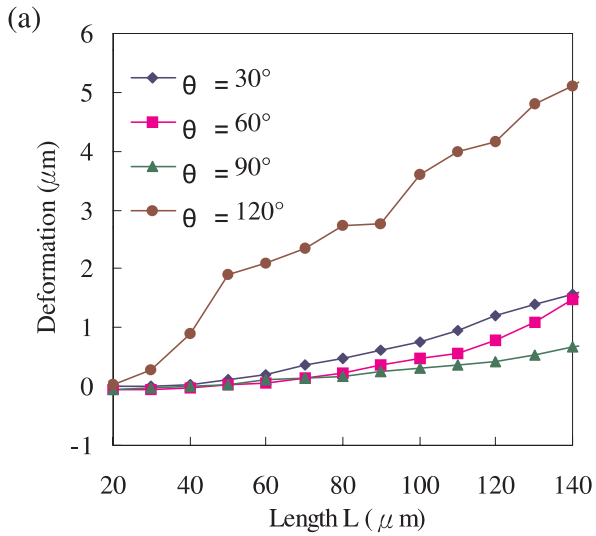

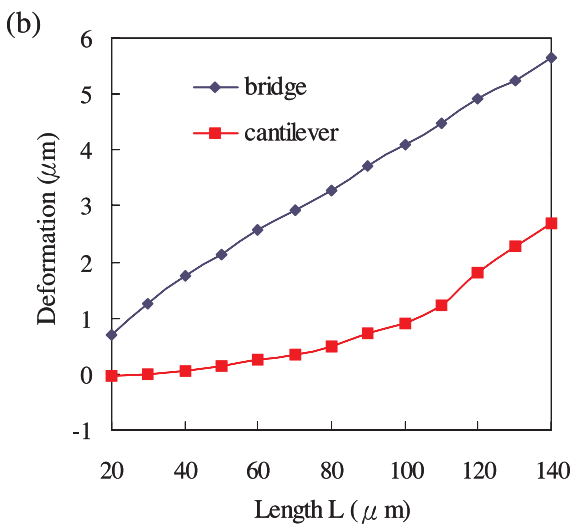

Figure 4. The variation of the deformation amplitude of a micromachined beam with the beam length L for (*a*) V-shaped beams with four different top angles, and (*b*) cantilevers and microbridges.

only limited research concerning the deflection of V-shaped beams caused by residual stress [8, 9]. This is mainly due to the complicated shape and boundary conditions of the V-shaped beam. Moreover, uncertain factors during the etching process make it more difficult to predict the deformation of such a microstructure caused by residual stress.

As illustrated in figure 1, the micromachined cantilever with $\theta = 0^\circ$ and the microbridge with $\theta = 180^\circ$ can be regarded as two limiting cases of the V-shaped beam. In the present study, the out-of-plane deformation of the V-shaped micromachined beam caused by residual stresses is investigated through experimental and analytical approaches. A finite element model was established to predict the effect of residual stresses on the V-shaped beam. An array of SiO_2 V-shaped microbeams with various lengths L, widths W, and top angles θ were fabricated and characterized as a study case. As demonstrated through the analytical and experimental results, the flatness of the V-shaped beam can be remarkably improved by changing its top angle.

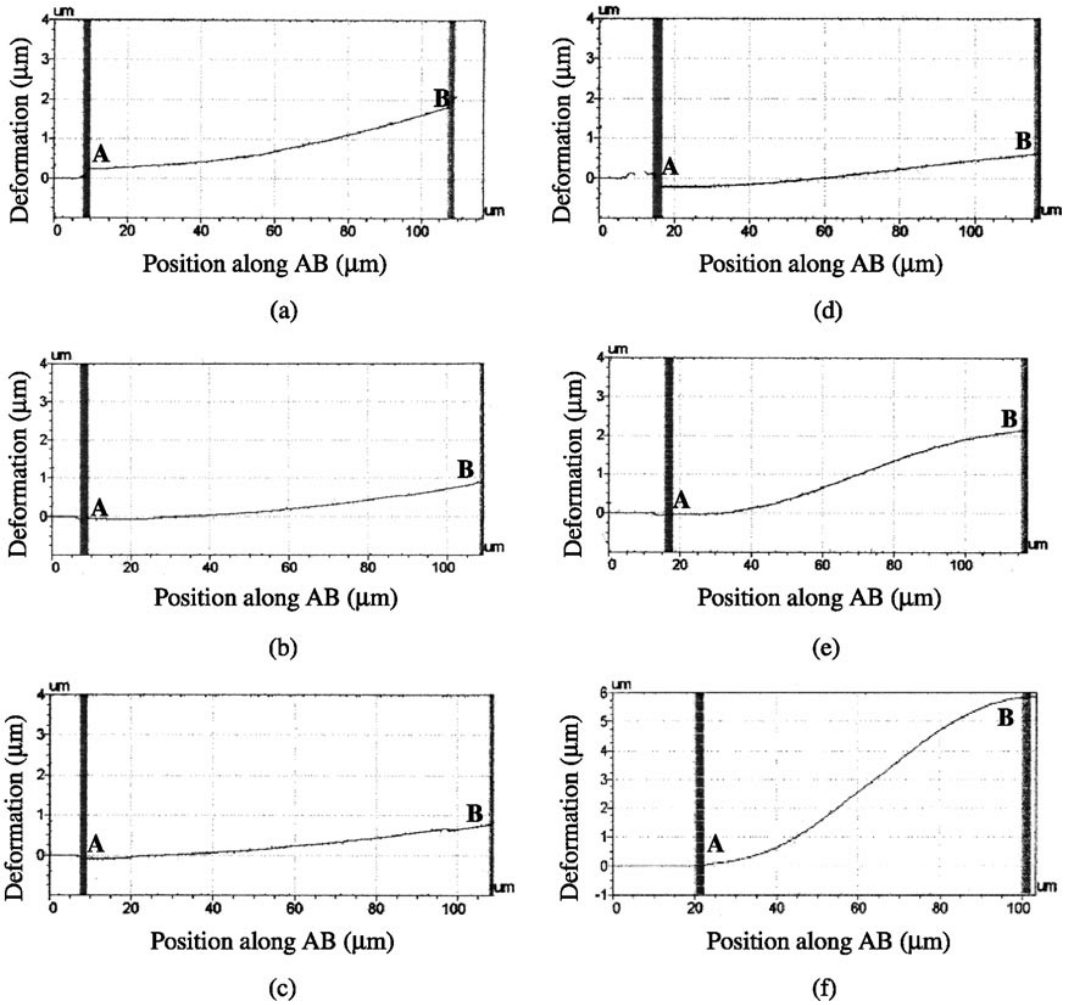

Figure 5. The measured deformation configuration of (*a*) cantilever, (*b*) $\theta = 30^\circ$ V-shaped beam, (*c*) $\theta = 60^\circ$ V-shaped beam, (*d*) $\theta = 90^\circ$ V-shaped beam, (*e*) $\theta = 120^\circ$ V-shaped beam, and (*f*) microbridge.

2. Experiment

The effect of residual stress on the deformation of different V-shaped micromachined SiO_2 beams was investigated in the experiment. The 1 μm thick V-shaped beams with various lengths L ($L = 20$–140 μm), three different widths ($W = 5$, 10, and 15 μm), and five different top angles ($\theta = 30^\circ$, 60°, 90°, 120°, and 150°) were fabricated. In addition, SiO_2 microbridges and microcantilevers, 5 μm in width and 20–140 μm in length, were also fabricated to compare their deflection with those of the V-shaped beams. A standard bulk micromachining process was used to fabricate these test beams. The residual stresses of the thermal SiO_2 film were exploited to deform the test beams. The (100) single-crystal Si substrate was placed in the furnace to grow a 1 μm thick thermal oxide layer at 1050 °C for 150 min. After the oxide layer was patterned, the substrate was etched anisotropically by KOH. The test beams were all released from the substrate after being etched for 10 min.

A scanning electron microscopy (SEM) photomicrograph of typical V-shaped micromachined beams of various lengths, L, and top angles, θ, is shown in figure 2. To determine the effect of residual stresses on the micromachined beams, the out-of-plane deformation of different beams was measured by means of non-contact interferometric profilometry. The out-of-plane deflection profile of the test beams shown in figure 3 was measured along the line AB in the experiment. Hence, the amplitude of deflection of the beams at point B was also determined. The measured amplitudes of deformation of the V-shaped beams of different lengths, L, and top angles, θ, are shown in figure 4(*a*). It is obtained that the deflection amplitude of the V-shaped beams gradually increases with the beam length when their top angles are $\theta \leqslant 90^\circ$. In addition, the deflection amplitude of the V-shaped beam decreases when the angle θ increases from 30° to 90°. However, the deflection amplitude of the V-shaped cantilevers remarkably increases with the beam length when $\theta = 120^\circ$. As shown in figure 4(*a*), the deflection amplitude of the V-shaped beam with $\theta = 120^\circ$ is several times greater than that with $\theta \leqslant 90^\circ$. This is apparently due to the buckling effect, and the V-shaped beam has a critical top angle θ_{cr}, with the beam length L and the beam thickness t specified. According to experiment, the critical top angle is $90^\circ < \theta_{cr} < 120^\circ$ when $L = 40$–140 μm and $t = 1$ μm.

The variation of the deflection amplitude with the beam length L for microcantilevers and microbridges was also

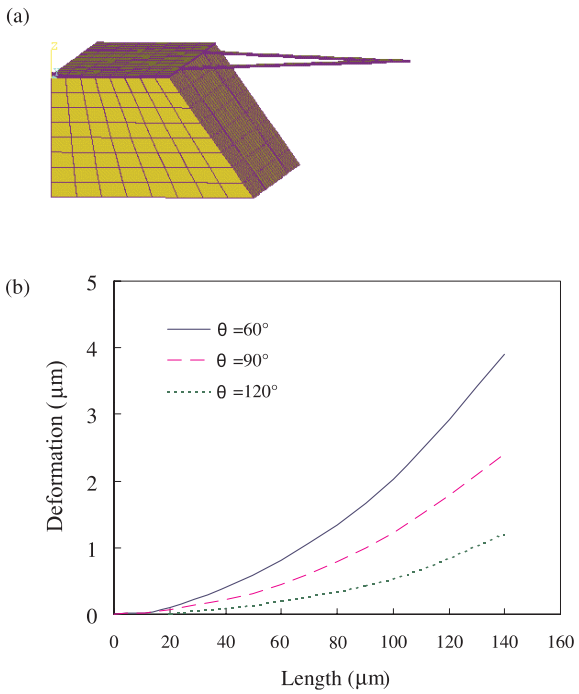

Figure 6. (*a*) The FEM model, and (*b*) the variation of the out-of-plane deflection at point B with the beam length L.

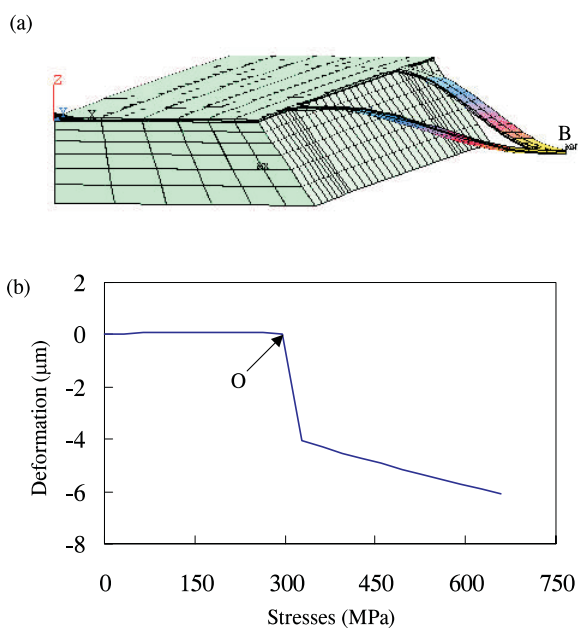

Figure 7. The FEM analysis results (*a*) the V-shaped beam buckled downward after being subject to the residual stresses and (*b*) the variation of the out-of-plane deflection at point B with the residual stresses.

measured, as shown in figure 4(*b*). The amplitude of deflection of the microcantilever gradually increases with the beam length as the beam was bent by the gradient residual stress [13]. However, the amplitude of deflection of the microbridge increases drastically with the beam length as the beam was buckled by the uniform compressive residual stress [14]. In conclusion, when subjected to residual stresses, the variation of the deflection amplitude with the beam length L of the

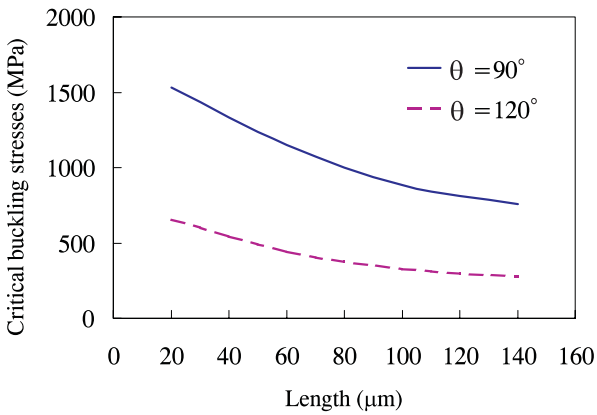

Figure 8. The variation of the beam length L with the critical buckling stress.

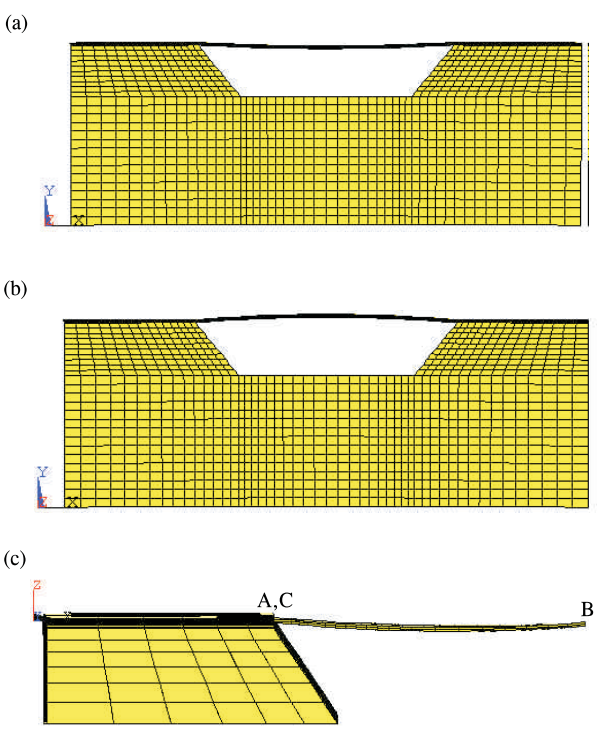

Figure 9. The initial (prebuckling) configuration of the micromachined beams (*a*) a microbridge subjected to the mean residual stress, (*b*) a microbridge subjected to the gradient residual stress, and (*c*) a V-shaped beam subjected to both mean and gradient residual stresses.

V-shaped beam with $\theta \leqslant 90^\circ$ is similar to that of the microcantilever. The variation of the deflection amplitude with the beam length L of the V-shaped beam with $\theta > 90^\circ$ is similar to that of the microbridge. The measured deflection profiles of the micromachined beams are also given, see figure 5. The lengths of the beams in figure 5 are all $L = 100$ μm, and the points A and B represent the positions of the beam indicated in figure 3. According to the results in figures 5(*b*)–5(*d*), it is again demonstrated that the deflection profiles of the V-shaped beam with $\theta \leqslant 90^\circ$ are similar to that of the cantilever ($\theta = 0^\circ$) shown in figure 5(*a*). On the other hand, the deflection profile of the V-shaped beam with $\theta > 90^\circ$ in figure 5(*e*) is similar to that of the microbridge ($\theta = 180^\circ$) shown in figure 5(*f*).

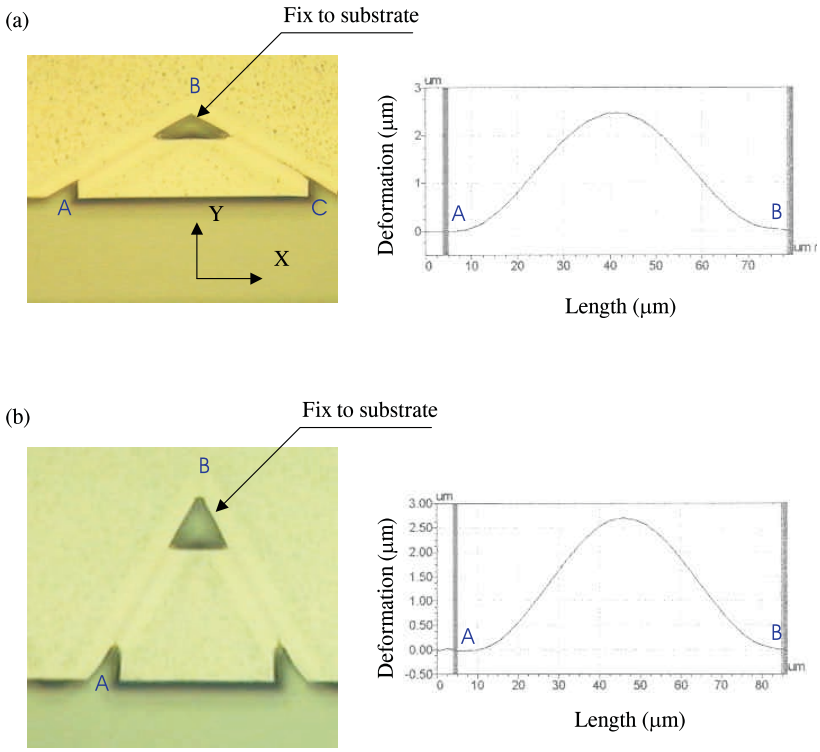

Figure 10. Photomicrograph and deformation configuration of the V-shaped beam after being undercut for 5 min (*a*) top angle $\theta = 60^\circ$ and (*b*) top angle $\theta = 120^\circ$.

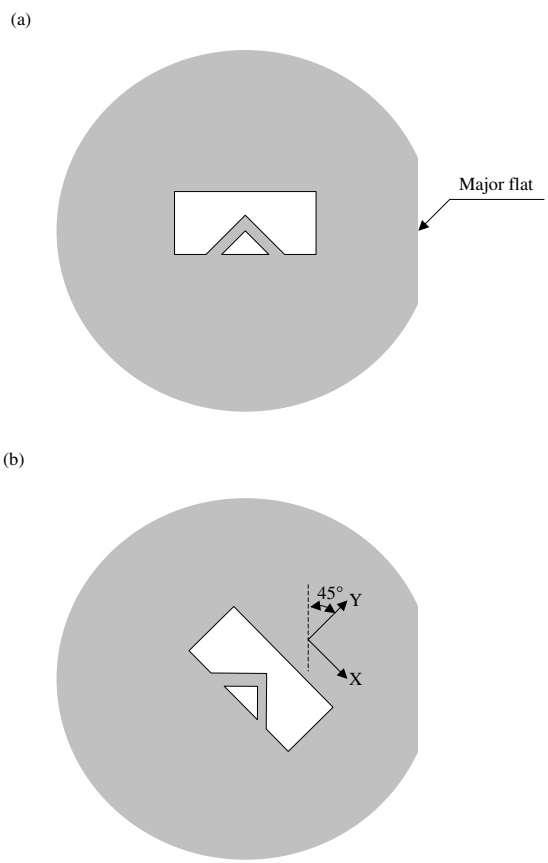

Figure 11. The V-shaped beam pattern aligned with the major flat of the substrate for (*a*) 0° and (*b*) 45°.

3. Analysis

To analyze the effect of residual stresses on the V-shaped micromachined beams, a three-dimensional finite element model, as shown in figure 6(*a*) was established. In the finite element model, the beam thickness t was specified; the variation of the out-of-plane deformation with θ and L will be discussed. In order to compare the analytical results with experiment, the thin-film material and the substrate employed in this model were SiO_2 and (100) single-crystal silicon, respectively. The bending of the V-shaped beam caused by the gradient residual stresses was discussed. The nonlinear analysis was also used to study the buckling behavior of the V-shaped beam caused by the mean residual stress. Consequently, the out-of-plane deformation configuration of the V-shaped beams resulting from the thin-film residual stresses can be predicted.

Figure 6(*b*) shows the variation of the beam length L and the out-of-plane bending deformation at point B for three different top angles θ. The out-of-plane deformation of the point B due to gradient residual stress decreases when the top angle increases. The typical nonlinear finite element method (FEM) result of the buckled V-shaped micromachined beam with a top angle $\theta = 120^\circ$ and beam length $L = 140$ μm is shown in figure 7. Figure 7(*a*) indicates that the V-shaped micromachined beam was buckled downward after being subjected to both mean and gradient residual stresses. Figure 7(*b*) shows the variation of the residual stress and the out-of-plane deflection of the beam. The critical buckling stress as indicated by point O in figure 7(*b*) is 280 MPa. The out-of-plane deflection of the beam is drastically increased

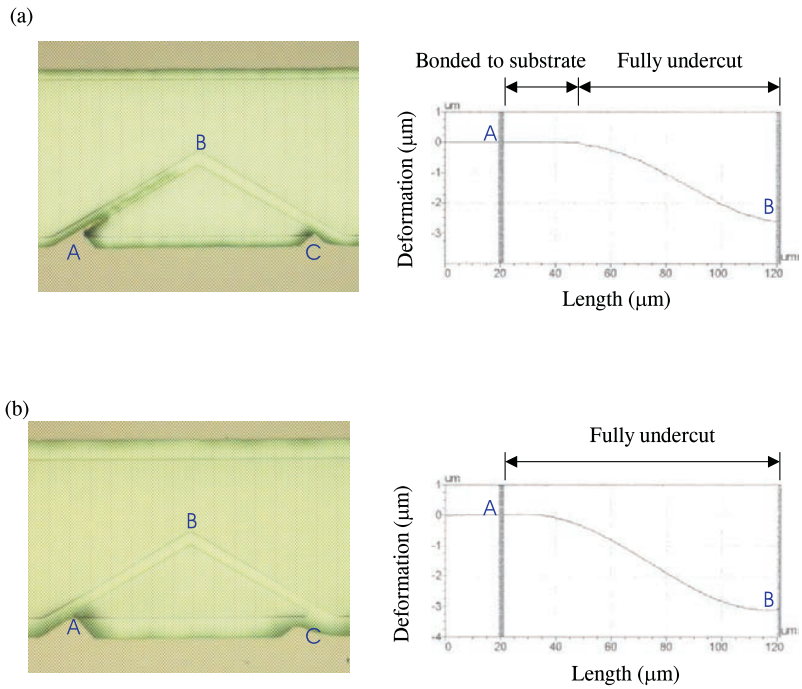

Figure 12. Photomicrograph and deformation configuration of the $\theta = 120^\circ$ V-shaped beam (aligned with the major flat of the substrate for 45°) after being undercut for (*a*) 5 min and (*b*) 10 min.

after the residual stress exceeds 280 MPa. According to the experiment, the critical top angle θ_{cr} of the V-shaped beam is between 90° and 120°. Therefore, the critical buckling stress of the beams with $\theta = 90^\circ$ and $\theta = 120^\circ$ was analyzed through the above approach. In figure 8, the full and broken curves represent the variation of the critical buckling stress with beam length for the beams with $\theta = 90^\circ$ and $\theta = 120^\circ$, respectively. From the analytical results it is found that the critical stress of the beam with $\theta = 90^\circ$ is much higher than that of the beam with $\theta = 120^\circ$. For instance when $L = 140$ μm, the critical buckling stress is only 280 MPa for the beam with $\theta = 120^\circ$, however the critical buckling stress becomes 750 MPa for the beam with $\theta = 90^\circ$.

The orientation of the buckling amplitude of a microbridge is significantly influenced by its initial configuration. As illustrated in figure 9(*a*), the initial configuration of the SiO_2 microbridge due to the partially clamped boundaries would lead the microbridge to buckle downwards [21]. As illustrated in figure 9(*b*), the initial configuration of the SiO_2 microbridge due to gradient residual stress would lead the microbridge to buckle upwards [21]. The microbridge tends to buckle upward if the gradient residual stress effect dominates the initial configuration; however, the microbridge tends to buckle downwards if the boundary effect dominates the initial configuration [21]. According to the FEM analysis, the initial configuration of the V-shaped beam due to the gradient residual stress and the boundary effect is shown in figure 9(*c*). This is due to the position of fixed ends A and C of the V-shaped beam. It is found that the initial configuration of the V-shaped beam caused by the two above effects is remarkably different from that of the microbridge. In summary, the V-shaped SiO_2 beam tends to buckle downwards under such an initial configuration, as shown in figure 9(*c*).

4. Discussion and conclusion

The characteristic of the V-shaped micromachined beam is dependent on the top angle θ. The microcantilever is regarded as a limiting case of the V-shaped beam with $\theta = 0^\circ$. Similarly, the microbridge is regarded as the other limiting case of the V-shaped beam with $\theta = 180^\circ$. Since the top angle θ ranges from 0° to 180°, the V-shaped beam can be regarded as a geometry transition structure from the microcantilever to the microbridge. Consequently, the V-shaped beam with a small θ can be used to prevent the structure from buckling. On the other hand, the beam with a large θ can be used to prevent the structure from bending. If one chooses the correct top angle of the V-shaped beam, the out-of-plane deformation of the microstructure can be minimized. In the study cases, the bending of the V-shaped beam was reduced by increasing its top angle. Moreover, the buckling problem needs to be considered when the top angle exceeds 90°. In summary, the optimal top angle in designing a flat V-shaped beam is $90^\circ < \theta < 120^\circ$.

In this study, the uniform residual stress of a thin film measured by the diagnostic micromachined cantilever technique was 300 MPa [13]. According to the FEM analysis, the V-shaped beam with a top angle $\theta = 120^\circ$ would not buckle unless $L > 140$ μm. However, the V-shaped micromachined beams with $\theta = 120^\circ$ and $L > 40$ μm all buckled in the experiment. There was a remarkable difference between the FEM analysis and the experiment. In addition, the FEM analysis predicted that a V-shaped micromachined beam subject to the mean and the gradient residual stresses would buckle downwards. On the contrary, the measured V-shaped micromachined beams buckled upwards, as shown in figure 5. It is believed that the difference between the experimental and analytical results is

mainly due to the ignorance of the undercut process in the FEM analysis. This will be demonstrated through the following experiment.

The photomicrographs in figure 10(*a*) and 10(*b*) show two SiO_2 V-shaped beams with $\theta = 60^\circ$ and 120°, respectively. According to the undercut process, the regions between AB and BC were initially fully undercut. The top of the V-shaped beam was still bonded to the substrate before the bulk etching process ended, as shown in figure 10. The dark region in figure 10 represents the area where the substrate has not been undercut. Apparently, the structure can be regarded as two microbridges before the V-shaped beam was fully suspended. In figure 10, the measured deflection profile of the region AB indicates that the microbridges all buckled upward. This buckling characteristic of the microbridge was discussed in [21]. Consequently, the V-shaped beam was induced to buckle upward after the substrate underneath was fully removed. Moreover, the V-shaped beam will be induced to buckle by the buckling microbridge when $L > 40$ μm, although the uniform residual stress may be smaller than the critical buckling stress.

An experiment was performed in this study to demonstrate the influence of the undercut process on the buckling of the V-shaped beam. In this experiment, a 1 μm thick thermal SiO_2 film was also grown on the (100) single-crystal silicon substrate. The pattern of the structures in figure 10 was aligned parallel to the major flat edge of the substrate as shown in figure 11(*a*). As shown in figure 11(*b*), the maximum etching rate of the substrate would occur in the y-direction during undercut when the pattern of the V-shaped beam was placed at 45° to the major flat edge of the substrate. The undercut of the V-shaped beam started from its top region; therefore, the formation of two buckled microbridges during the etching process shown in figure 10 was prevented. The photomicrographs in figure 12 show the undercut of an $L = 100$ μm and $\theta = 120^\circ$ V-shaped beam at various etching times. From the photomicrographs in figure 12(*a*) it was found that the top of the V-shaped beam was fully undercut after etching for 5 min. The measured deflection profile of the beam in figure 12(*a*) indicated that it was only undercut for 60 μm, and it buckled downwards. When the etching time increased to 10 min, the V-shaped beam was fully undercut, as shown in figure 12(*b*), and it remained buckled downwards. This phenomenon agrees with that of the FEM analysis in figure 7; it shows that traditional solid mechanics analysis may not accurately predict the deformation of microstructures caused by residual stresses if the fabrication processes are ignored.

Acknowledgments

This material is based (in part) upon work supported by the National Science Council (Taiwan) under Grant NSC 89-2218-E007-011. The author would like to express his appreciation to the NSC Central Regional MEMS Research Center (Taiwan), and NSC Precision Instrument Development Center (Taiwan) in providing fabrication facilities.

References

[1] Emmenegger M, Taschini S, Korvink J G and Baltes H 1998 Simulation of a thermomechanically actuated gas sensor *Proc. 11th Ann. Int. Workshop on MEMS (Heidelberg, Germany)* pp 184–9

[2] Tao X, Guoying W, Guobing Z, Wei W and Ting L 2000 A novel micro gas sensor with high selectivity based on both mass and conductivity measurement *Proc. 13th Ann. Int. Conf. on MEMS (Miyazaki, Japan)* pp 108–13

[3] Sader J E, Larson I, Mulvaney P and White L R 1995 Method for the calibration of atomic force microscope cantilevers *Rev. Sci. Instrum.* **66** 3789–98

[4] Volklein F and Baltes H 1992 A microstructure for measurement of thermal conductivity of polysilicon thin films *J. Microelectromech. Syst.* **1** 193–6

[5] Eron H K, Richard J R and Gregory T A 1995 Diode-based thermal RMS converter with on-chip circuitry fabricated using standard CMOS technology *Proc. 8th Int. Conf. on Solid-State Sensors and Actuators and Eurosensors IX (Stockholm, Sweden)* vol 1, pp 154–7

[6] Kimura M, Toshima K and Satoh H 1999 Optical vibration and acceleration sensor with a silicon cantilever 1999 *1999 ASME Int. Mechanical Engineering Congress and Exposition (Nashville, TN)* vol 1, pp 117–21

[7] Strandman C and Backlund Y 1997 Bulk silicon holding structures for mounting of optical fibers in V-grooves *J. Microelectromech. Syst.* **6** 35–40

[8] Liu C and Gamble R 1998 Mass-producible monolithic silicon probes for scanning probe microscopes *Sensors Actuators* A **71** 233–7

[9] Sader J E and White L 1993 Theoretical analysis of the static deflection of plates for atomic force microscope applications *J. Appl. Phys.* **74** 1–9

[10] Tortonese M 1997 Cantilevers and tips for atomic force microscope *IEEE Eng. Medicine Biology* **162** 28–33

[11] Benrakkad M S, Lopez-Villegas J M, Samitier J and Kirsen M 1995 Stress gradient and structural properties of atmospheric and reduced pressure deposited polysilicon layers for micromechanical sensors *Sensors Actuators* A **51** 9–12

[12] Guckel H, Burns D, Rutigliano C, Lovell E and Choi B 1992 Diagnostic microstructures for the measurement of intrinsic strain in thin film *J. Micromech. Microeng.* **2** 86–95

[13] Fang W and Wickert J A 1996 Determining mean and gradient residual stresses in thin films using micromachined cantilevers *J. Micromech. Microeng.* **6** 301–9

[14] Fang W and Wickert J A 1994 Post buckling of micromachined beams *J. Micromech. Microeng.* **4** 116–22

[15] Ding X, Ko W H and Mansor J M 1990 Residual stress and mechanical properties of boron-doped p^+-silicon films *Sensors Actuators* A **21** 866–71

[16] Yacobi B G and Sheldon P 1990 Analysis of stress variation in epitaxial using cathodoluminescence microscopy and spectroscopy *Mater. Res. Soc.* **188** 47–52

[17] Chou C S, Shie J S and Chen C N 1997 Fabrication of low-stress dielectric thin-film for microsensor applications *IEEE Electron Device Lett.* **18** 599–601

[18] Volklein F 1990 Thermal conductivity and diffusivity of a thin film SiO_2–Si_3N_4 sandwich system *Thin Solid Films* **188** 27–33

[19] Chen Y 1997 The fabrication and discussion of silicon nitride membranes by chemical vapour deposition *Masters Thesis* National Chiao Tung University, Taiwan

[20] Chu W H and Mehregany M 1993 A study of residual stress distribution through the thickness of P^+ silicon film *IEEE Trans. Electron Devices* **40** 1245–50

[21] Fang W, Lee C H and Hu H H 1999 On the buckling behavior of micromachined beams *J. Micromech. Microeng.* **9** 236–44